Anisotropy At The South Chilean Active Continental Margin?

Wolfgang Soyer

Fachrichtung Geophysik, FU Berlin, Malteserstrasse 74-100, 12249 Berlin
(w.soyer@geophysik.fu-berlin.de)

Introduction

Within the framework of the SFB267 "Deformation Processes in the Andes", at the end of 2000 a long period electromagnetic survey was carried out in South Chile, where data were collected along two parallel profiles plus two additional sites further south to check for eventual along-strike variations of electrical conductivity (figure 1). *Brasse and Soyer* [2001] present a first analysis and modelling of the magnetotelluric data set, which revealed moderately enhanced conductivities ($\sim$10 Ωm) in 20 – 40 km depth below and east of the volcanic arc, where the trench-parallel Liquiñe-Ofqui Fault intersects the two profiles. As in north Chile ($\sim$21°S), no conductivity anomalies in direct relation to the subducting Nazca plate could be detected, which according to numerical studies is — at least with onshore data alone — principally problematic due to the dominant coast effect, which masks inductive responses from deeper seated targets (*Evans et al.* [2002]). In the study area, the preferred magnetotelluric strike direction roughly matches the expected structural strike, and a regional skew of < 0.3 (after Bahr) for most of the impedance data seems to justify the isotropic 2-D approach shown there, which reproduces the off-diagonal impedance data. An analysis of geomagnetic variation data, however, clearly evinces, that within the study area a dimensionality greater than (isotropic) 2-D is observed.

Local geomagnetic data

Applying the program package from *Egbert and Booker* [1986], local geomagnetic bivariate transfer functions of 34 deployed field stations were calculated for the period range of 10 s to $2{\cdot}10^4$ s, in figure 2 presented as induction vectors (IV) for the periods 100 s and 3300 s:

$$B_z = T_x B_x + T_y B_y$$

$$\Re(IV) = \Re(T_x)\mathbf{e}_x + \Re(T_y)\mathbf{e}_y \qquad \Im(IV) = \Im(T_x)\mathbf{e}_x + \Im(T_y)\mathbf{e}_y.$$

(Wiese convention). In southern Chile at 39° S, declination is about N9°E, which turned out to be roughly the structural strike deduced from magnetotelluric tensor analysis, and has to be considered in the presentation of these vectors.

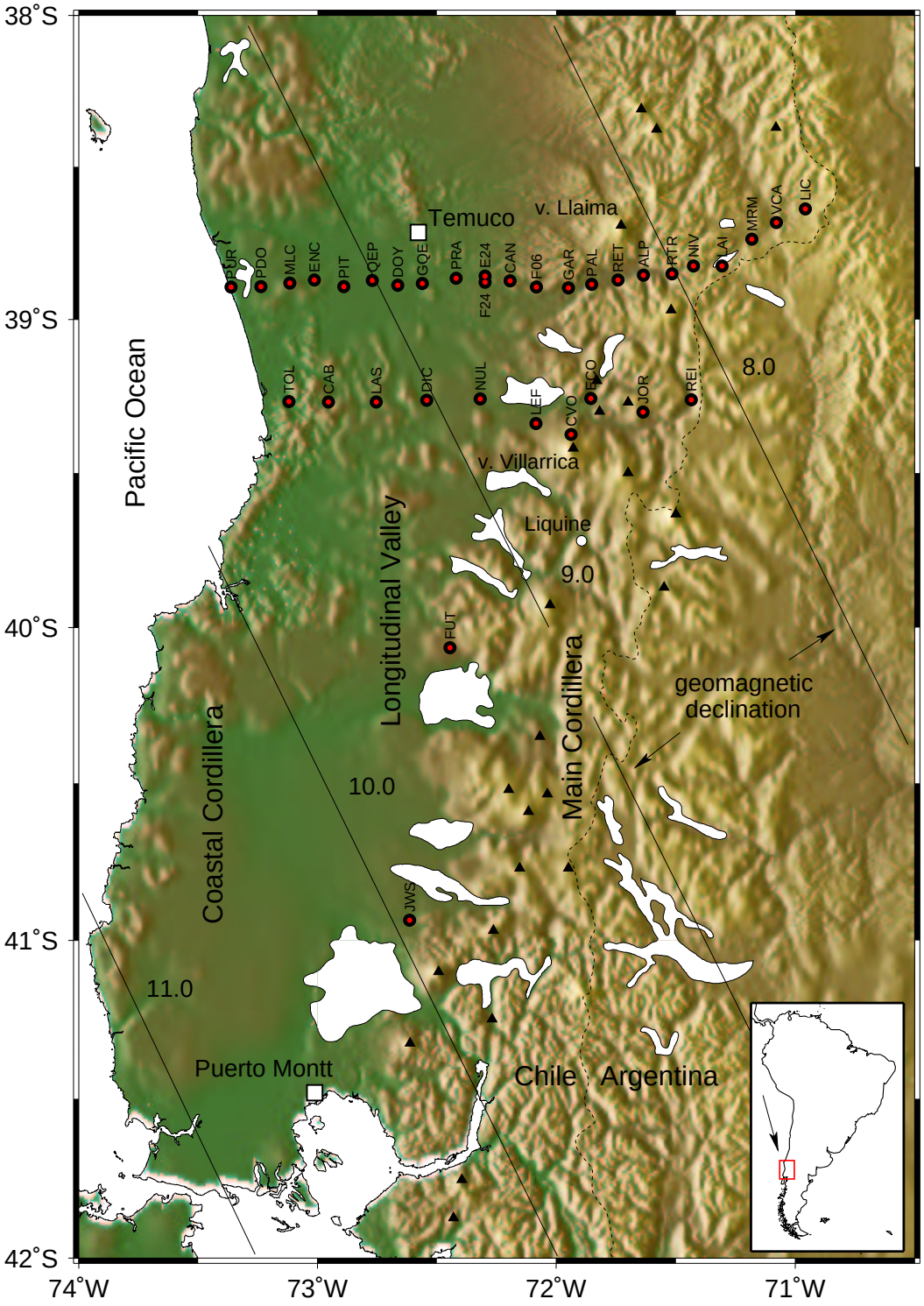

Figure 1: Study area and site locations from the year 2000 campaign in the southern Andes. Stations are aligned along two profiles. The main profile along ∼ 39°S with a length of 210 km comprises 22 stations. Roughly 40 km further south, another 10 stations compose a second line, which is about 145 km long. The isolines of equal declination were calculated from International Geomagnetic Reference Field coefficients (IGRF 2000). Holocene volcanoes are marked by triangles.

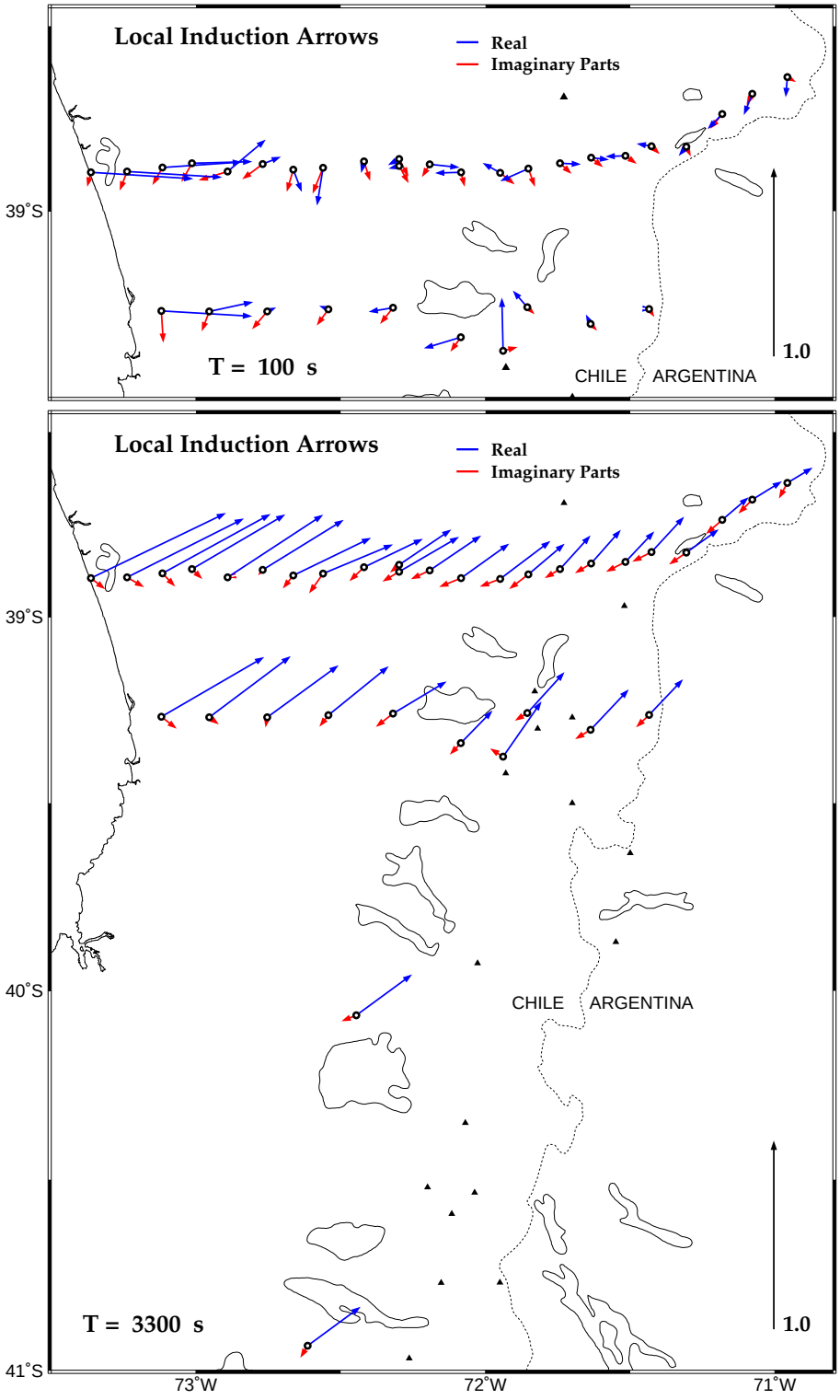

Figure 2: Induction arrows for the periods 100 s and 3300 s. Triangles represent quaternary volcanoes. Note that some tens of kilometers offshore from the coast, the sea is very shallow (about 100 m), and the axis of the ≈4 km deep trench runs in ∼N9° E direction.

At 100 s, the inductive effect of the Pacific ocean is visible only at the westernmost stations. Arrows at the remaining sites are short and indicate no major conductivity contrast, though at the eastern part of the study area they point preferably towards west, indicating increasing conductivities to the east. The fields at the southernmost station of the southern profile (CVO) close to Villarrica volcano is clearly influenced by enhanced conductivities just below the volcano. At longer periods, there is obviously no structure in the east that is conductive enough to compensate the ocean effect.

Instead, arrows at all stations towards longer periods get a significant N-S component, with a maximum at about 4 to 6 $\cdot 10^3$ seconds. Figure 2 illustrates, how uniformly this is observed throughout the study area. For some stations, the N-S component even exceeds the E-W component. Assuming only isotropic conductivities, this would be a clear hint at enhanced conductivities to the south. To check this, two additional stations were deployed in the Longitudinal Valley 70 (FUT) and 140 (JWS) kilometers further south, in a roughly equal distance from the deep sea. Their local induction vectors are very similar to those of the corresponding stations from the north. This is best illustrated in figure 3: the geomagnetic north component T_x of the local induction vectors from the three stations F06, FUT and JWS, which together comprise a N-S distance of ∼230 km, plotted side by side, especially at longer periods shows marginal lateral variation along the strike direction of the land-sea contrast. This strongly suggests that the observation might be explainable by 2-D modelling including (at least) horizontally anisotropic structures with an anisotropy strike $\alpha \neq 0$ with respect to the structural strike.

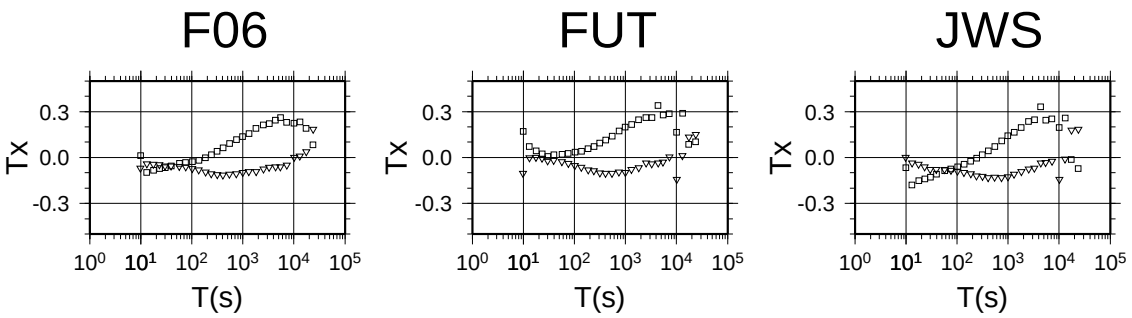

Figure 3: The geomagnetic north component T_x of local induction vectors (rectangles: real parts, triangles: imaginary parts) as a function of period comprises little change along strike (N-S distance between F06 and JWS: ∼230 km, see figure 1).

Anisotropy at a land-sea contrast

Allowing for anisotropy, the conductivity σ becomes a tensor, which, on account of the demanded nonnegativity of the time-averaged specific energy dissipation $\frac{1}{2}\mathbf{E}^*\mathbf{j} = \frac{1}{2}\mathbf{E}^*\boldsymbol{\sigma}\mathbf{E}$, is positive semidefinite (in conductors positive definite), and, as purely ohmic conduction is considered, symmetric:

$$\boldsymbol{\sigma} = \begin{pmatrix} \sigma_{xx} & \sigma_{xy} & \sigma_{xz} \\ \sigma_{xy} & \sigma_{yy} & \sigma_{yz} \\ \sigma_{xz} & \sigma_{xy} & \sigma_{zz} \end{pmatrix}$$

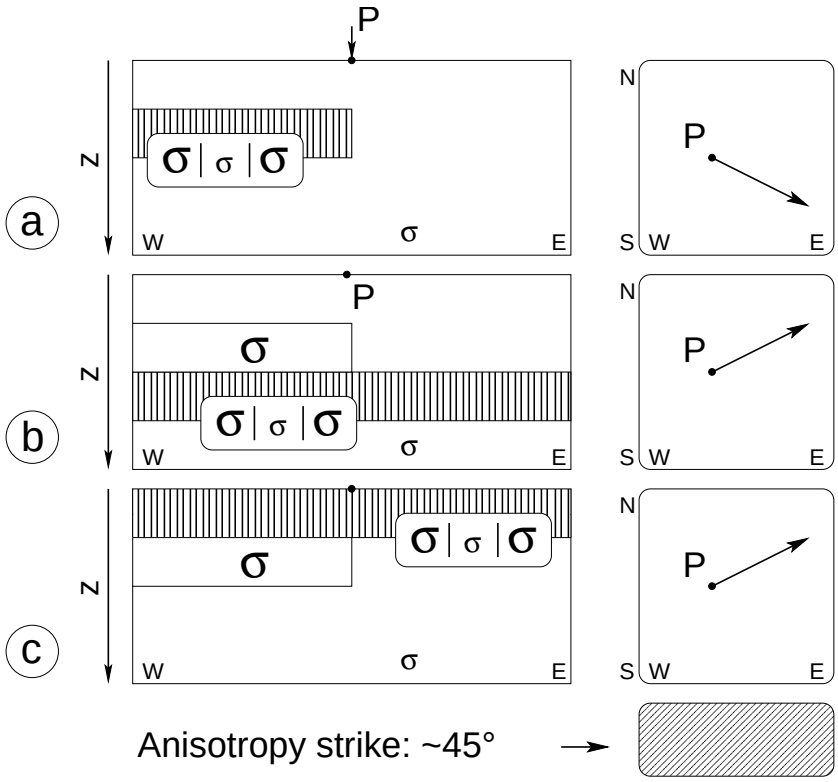

Figure 4: The deviation of local induction vectors at 2-D structures due to horizontal anisotropy of strike $\alpha > 0$, sketched from results of Pek and Verner [1997]. Left: side view on three 2-D models, all comprising anisotropic structures, which's anisotropy is equivalent with good conducting vertical lamellae, horizontally rotated by an angle α (patched structures). Sizes of the character σ reflect the values of the respective (principal) conductivities. Right: Induction vectors at point P above the conductivity contrast. Vector deviations of model b and c are only qualitatively comparable, i.e. deviation is towards the same direction, but the effect is maximal at different periods.

Such a tensor can be represented by three principal values and three rotation angles, i.e. from any coordinate system, the tensor can be transformed into diagonal form by three successive rotations (principal axis transformation). Like for isotropic 2-D conductivity distributions, only currents along the structural strike contribute to the vertical magnetic field component.

In the following considerations, only the horizontal strike angle α, i.e. the rotation angle by which the system of principal axes is rotated around the vertical axis with regard to the structural strike direction, is unequal zero. Therefore, the principal conductivities will be referred to in the following with $\sigma_\parallel$, $\sigma_\perp < \sigma_\parallel$ (both in horizontal direction) and σ_z, and the tensor in structural coordinates becomes:

$$\boldsymbol{\sigma} = \begin{pmatrix} \sigma_\parallel \cos^2\alpha + \sigma_\perp \sin^2\alpha & (\sigma_\parallel - \sigma_\perp)\sin\alpha\cos\alpha & 0 \\ (\sigma_\parallel - \sigma_\perp)\sin\alpha\cos\alpha & \sigma_\parallel \sin^2\alpha + \sigma_\perp \cos^2\alpha & 0 \\ 0 & 0 & \sigma_z \end{pmatrix}$$

A modelling approach controlled by intuition which is based on experiences with isotropic structures will inevitably result in attempts to fit the data with anisotropy strikes roughly perpen-

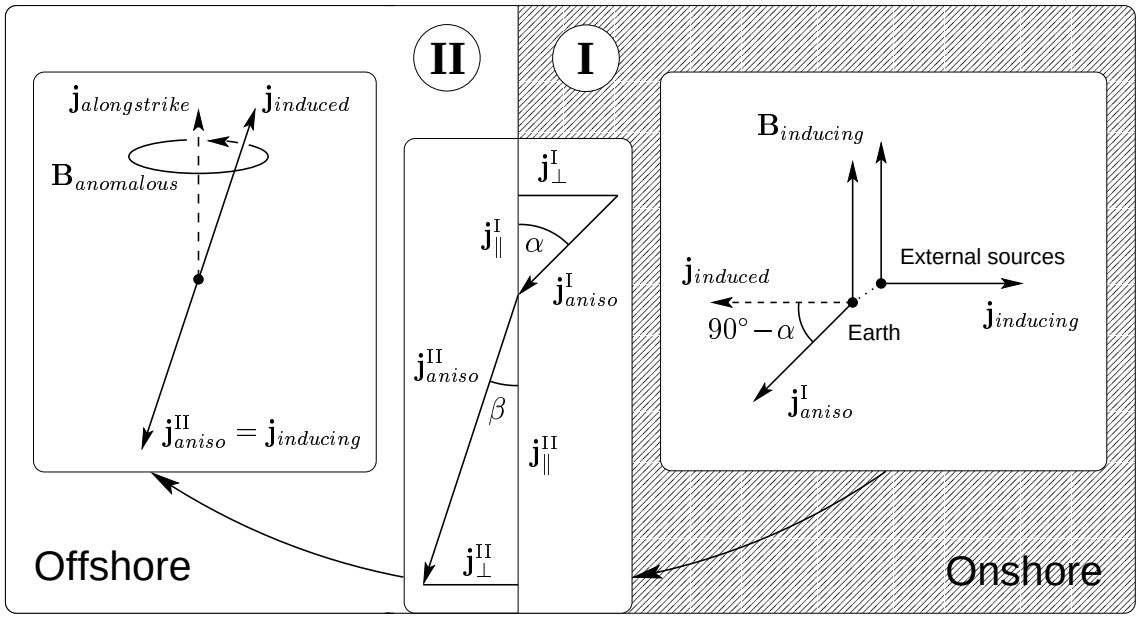

Figure 5: Sketch to explain the relation between B_z and B_x at a sea | anisotropic land contrast (after Weidelt [1999], modified for this specific setting). Onshore anisotropy is equivalent with well-conducting vertical lamellae of strike α. Secondary currents onshore, induced by an external magnetic field parallel to the strike direction, are deflected towards the better conducting direction (I). "Secondary secondary" currents, the ocean's response to from land incident secondary fields, due to the refraction at the structural boarder are mainly oriented along strike. Note that only the along strike component of the currents contributes to an anomalous magnetic field at the earth's surface, which is positive downward on land. The total *current density in the ocean results in a current flow in north-west direction.*

dicular to induction vectors. Model studies performed by *Pek and Verner* [1997], *Weidelt* [1999] and *Beike* [2001], however, make clear that this will work only in specific cases. Figure 4 qualitatively summarizes some results presented in *Pek and Verner* [1997] for simple 2-D conductivity distributions with anisotropic structures, which's anisotropy is equivalent with vertical conductive lamellae that are rotated by an anisotropy strike α. In cases where the 2-D contrast is based on a highly anisotropic structure itself, induction arrows are deflected against the direction of the preferred conductivity, as expected (model *a*). In contrast, if an isotropic 2-D conductor is coupled with an extended anisotropic body, induction arrows are rotated *into the anisotropy strike direction* (model *b* & *c*). This phenomenon has equivalently been observed by *Weidelt* [1999][1].

Though at first glance rather surprising, this observation is indeed understandable. *Pek and Verner* [1997] presented plots of horizontal current densities for both polarizations, calculated for a model as given in figure 4c. For an inducing regional (concerning the structural strike) TE-polarization, the deflection of currents towards west (i.e. left) in the anisotropic layer does not entail a significant current density component perpendicular to the structural strike in the

[1] *Weidelt* [1999] states: "This is, in fact, a quite general phenomenon that occurs whenever an elongated (isotropic) conductor is embedded in an anisotropic host whose horizontal axes do not coincide with those of the elongated conductor."

isotropic layer below. The northward deflection of currents in the anisotropic overburden, which is excited by a inducing regional TM-polarization, however, leads to a strong south component of the currents within the isotropic conductor. The clue to the understanding of this phenomenon is to regard the fields of the secondary currents, that are induced in the anisotropic structure by an inducing regional TM-polarization, as inducing fields that are incident on the isotropic conductor. The sketch in figure 5 illustrates this interpretation for the case of the 2-D contrast: anisotropic land with $\alpha > 0$ | (isotropic) sea. The onshore induced currents $\mathbf{j}^{\mathrm{I}}_{aniso}$ are deflected by the angle $90° - \alpha$ towards the direction of the well-conducting lamellae. Due to the refraction law for currents

$$\frac{j^{\mathrm{I}}_{\parallel}}{j^{\mathrm{II}}_{\parallel}} = \frac{\sigma_{\parallel}}{\sigma_{sea}} = \frac{\tan\beta}{\tan\alpha}$$

(comp. figure 5. Here, σ_{sea} is the conductivity of sea water, and $\sigma_{\parallel}$ is the preferred conductivity of the anisotropic half-layer), almost for any realistic conductivity of the well-conducting lamellae, the inducing secondary currents $\mathbf{j}^{\mathrm{II}}_{aniso}$ are strongly deflected towards the structural strike ($\sigma_{\parallel} \ll \sigma_{sea} \rightarrow \beta \ll \alpha$), and so do the oppositely directed induced currents in the ocean. The anomalous magnetic field of the latter currents then has a positive downward component onshore which can be observed far inland. Thus, an inducing TM-polarization here leads to a positive vertical magnetic field, which means that $T_x > 0$, respectively that induction arrows point northward. As this would just be the opposite for $\alpha < 0$, we can infer that an anisotropic structure adjoining the Pacific ocean in south Chile accounts for the observed north deviation of induction arrows, then its strike is positive in a clockwise rotational sense.

Anisotropic 2-D modelling

It can be concluded that the investigation of an anisotropic structure close to the ocean only in terms of geomagnetic transfer functions is best undertaken by concentrating on the geomagnetic north component T_x of the induction arrows in a 2-D anisotropic modelling study.

The here employed finite difference code from *Pek and Verner* [1997] calculates responses of 2-D conductivity distributions with arbitrary anisotropy for any element of the model (see there for any details on the code). In this modelling study, only the horizontal strike α, together with the three principal conductivities is regarded as a free parameter. The models are discretized by 158 rows and 61 columns plus 10 air layers for the TE-mode. Sea water conductivity has been set to $0.27\,\Omega$m. The shape of the subducting Nazca plate is deduced from hypocenter locations of local earthquake data, which were recently recorded in a seismic network (*Bohm et al.* [2002]).

When modelling anisotropic structures (if additionally a reduced data set of just one type of transfer function is modelled) it is particularly difficult to be sure that the range of models has been exploited sufficiently. Still, it has been found that the data could only be explained by models of the *type* shown in figure 6. The only anisotropic structure of these models is a continental layer with an upper boundary in the mid crust and the integrated conductivities $\tau_{\parallel} \approx 800\,\mathrm{S}$ and $\tau_{\perp} \lesssim 30 \cdot \tau_{\parallel}$. The anisotropy strike α is positive from geomagnetic north, somewhere between ∼15 and ∼60 degrees; best results have been obtained with $\alpha \approx 30°$. For this model, geomagnetic responses are completely insensitive to the vertical conductivity σ_z,

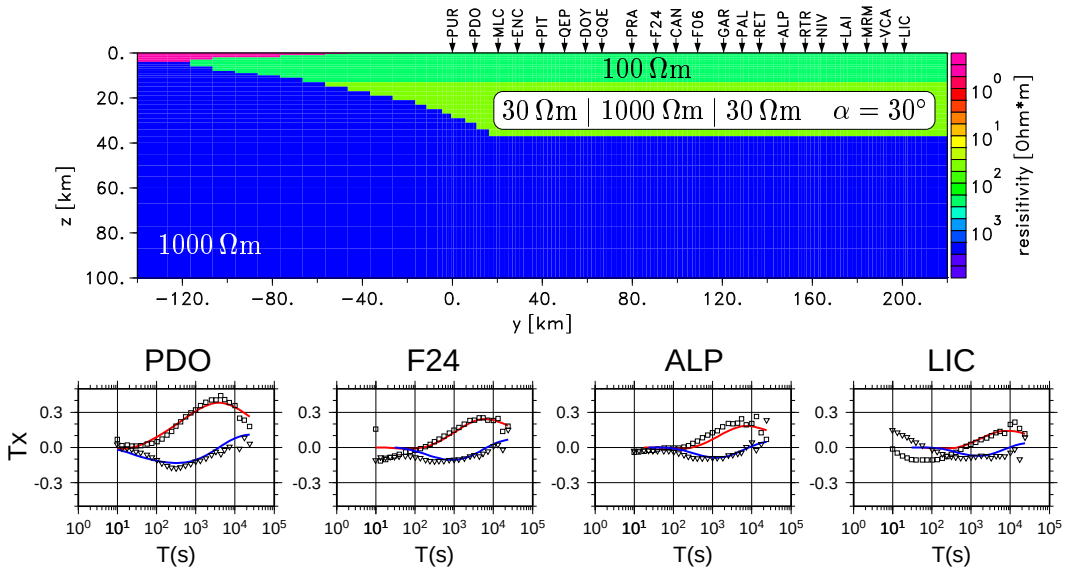

Figure 6: An anisotropic model for south Chile, which is preferred due to results from the isotropic 2-D modelling, and its response (T_x, i.e. the along strike component of induction vectors) from west to east at four stations (rectangles: real parts, triangles: imaginary parts). Between 13 km and 27 km depth, the model comprises an anisotropic continental layer with anisotropy strike $\alpha = 30°$ with respect to the structural strike, and the principal resistivities $\rho_{\|} = 30\,\Omega m$, $\rho_{\perp} = 1000\,\Omega m$ and $\rho_z = 1000\,\Omega m$ (see text for discussion).

so that $\sigma_z = \sigma_{\|}$ and $\sigma_z = \sigma_{\perp}$ yield comparable responses. This layer must be covered by a moderately conductive isotropic layer to ensure that $T_x \approx 0$ at short periods. Below the anisotropic layer, resistivities have to be high ($\gtrsim$1000 Ωm). Distinct from the sketch described above, the anisotropic structure has no direct contact with the Pacific ocean, which is obviously not necessary to account for the phenomenon of along strike oceanic currents that are induced by an inducing regional TM polarization.

In figure 7, four alternative models with certain changes with regard to the 'preferred' model of figure 6 are shown. The thickness of the anisotropic layer in model *a* is reduced to a third (i.e. 8 km), while the principal conductivity $\sigma_{\|}$ is enhanced by a factor of three (i.e. 0.1 S/m), thus the integrated conductivity $\tau_{\|}$ being unchanged. The response of this model resembles that of the model in figure 6. In model *b*, the eastern part of the anisotropic layer is replaced by an anisotropic conductor of 10 Ωm to account for the enhanced conductivities found there in the isotropic inversion shown in *Brasse and Soyer* [2001]. This leads to an effect equivalent to the interaction anisotropic layer – ocean, but oriented in the other direction, opposing the former. In contrast, toward east increasing conductivities maintaining the anisotropy sustain the effect, making it even too strong (not illustrated; this is qualitatively a positive superposition of the effects shown in 4a and 4b,c). Surprisingly, decreased resistivities (here: 10 Ωm instead of 1000 Ωm) in the oceanic crust and *upper* oceanic lithosphere do not significantly change onshore responses (model *c*). If, however, the conductivity of the complete oceanic lithosphere is enhanced, responses are significantly smaller and shifted towards shorter periods (model *d*).

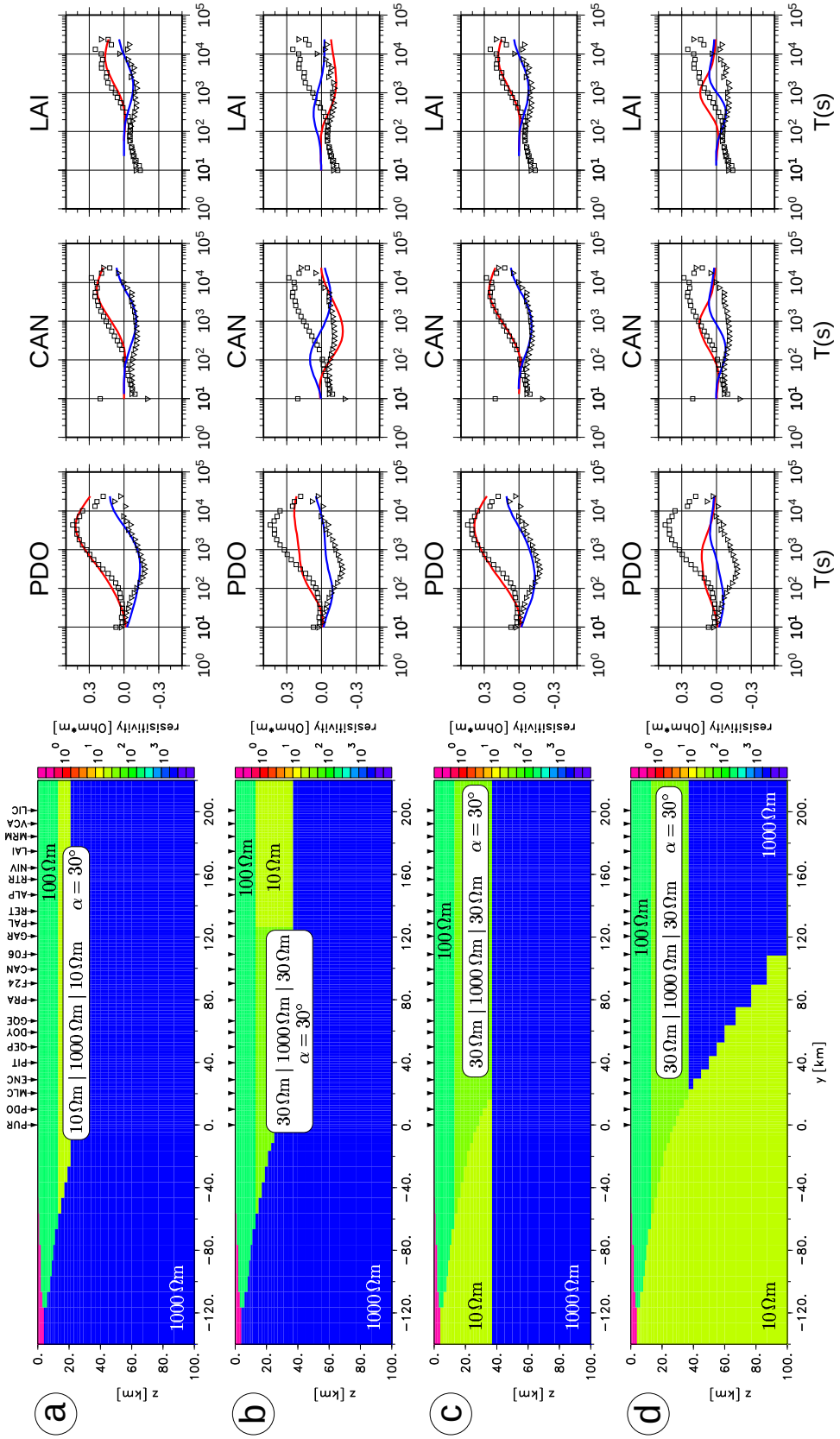

Figure 7: Four anisotropic 2-D models for the southern Andes, each with specific changes from the 'preferred' model in figure 6, and its responses (along strike induction vector component T_x at three selected stations from west to east). Resistivities in the round boxes refer to the principal resistivities $\sigma_{\|}$, $\sigma_{\perp}$ and σ_z. In all models, the anisotropy strike α is 30 degrees.

Conclusions and outlook

Discovering electrical anisotropy from an analysis of geomagnetic variation data is bound to a lateral conductivity contrast which's strike does not match the anisotropy strike. The sharper the contrast, the stronger is the signature of anisotropy within the data. The enormous land-sea contrast, in isotropic electromagnetic respects clearly regarded as an obstruction, is thus an ideal environment for the discovery of continental anisotropy, particularly at active continental margins, where tectonic forces presumably accounting for anisotropy are especially high. In south Chile, the actual convergence direction of subduction is N77°E, which is unlikely to be in the range of possible strikes of anisotropy or perpendicular to it. Cenozoic faults in the Longitudinal Valley and the volcanic arc region, as well as the principal compressional stress direction σ_1 of quaternary tectonic events are oriented in NE-SW direction (*Lavenu and Cembrano* [1999]).

The disagreement of the anisotropic modelling with the isotropic modelling presented in *Brasse and Soyer* [2001] is ocular. Also, the component of the induction vector perpendicular to the structural strike is not explained by this modelling. It is suggested, that results from both approaches reflect important aspects of the true conductivity distribution, and the task of further, necessarily anisotropic 2-D and/or 3-D modelling is to deduce *one* electrical image of the subsurface that is consistent with all types of data, impedance and pure geomagnetic transfer functions.

References

Beike, J., Studien zur anisotropen Leitfähigkeitsverteilung und ein Versuch zur Erklärung magnetotellurischer Übertragungsfunktionen in der Küstenkordillere Nordchiles, Diplomarbeit, Institut für Geologie, Geophysik und Geoinformatik, FU Berlin, 2001.

Bohm, M., S. Lüth, G. Asch, K. Bataille, C. Bruhn, A. Rietbrock, and P. Wigger, The Southern Andes between 36° and 40°S latitude: seismicity and average velocities, *Tectonophysics*, *submitted*, 2002.

Brasse, H., and W. Soyer, A magnetotelluric study in the Southern Chilean Andes, *Geophysical Research Letters*, *28 (19)*, 3757–3760, 2001.

Egbert, G. D., and J. R. Booker, Robust estimation of geomagnetic transfer functions, *Geophysical Journal of the Royal Astronomical Society*, *87*, 173–194, 1986.

Evans, R. L., A. D. Chave, and J. R. Booker, On the importance of offshore data for magnetotelluric studies of ocean-continent subduction systems, *Geophysical Research Letters*, *accepted*, 2002.

Lavenu, A., and J. Cembrano, Compressional- and transpressional-stress pattern for Pliocene and Quaternary brittle deformation in fore arc and intra-arc zones (Andes of Central and Southern Chile, *Journal of Structural Geology*, *21*, 1669–1691, 1999.

Pek, J., and T. Verner, Finite difference modelling of magnetotelluric fields in 2-D anisotropic media, *Geophysical Journal International*, *128*, 505–521, 1997.

Weidelt, P., 3-D conductivity models: implications of electrical anisotropy, in *Three-Dimensional Electromagnetics*, edited by M. Oristaglio and B. Spies, pp. 119–137, SEG, Tulsa, 1999.